1- and 2-Dimensional Tungsten-183 and Vanadium-51 NMR Characterization of Isopolymetalates and Heteropolymetalates

Peter J. Domaille

Contribution No. 3493 from the Central Research and Development Department, E. I. du Pont de Nemours & Company, Wilmington, Delaware 19898. *Received May 21, 1984*

Abstract: 1- and 2-dimensional (2-D) ^{183}W NMR techniques are applied to establishing the structures of several series of vanadotungstates. 2-Dimensional connectivity patterns of $[PVW_{11}O_{40}]^{4-}$, $[SiVW_{11}O_{40}]^{5-}$, and $[BVW_{11}O_{40}]^{6-}$, obtained with the 2-D INADEQUATE pulse sequence, unambiguously establish they are based on the α-Keggin structure. Specific positional isomers, α-1,2-$[XV_2W_{10}O_{40}]^{n-}$ and α-1,2,3-$[XV_3W_9O_{40}]^{(n+1)-}$ (X = Si, P; n = 5, 4), are also synthesized and their structures established from the 2-D connectivity pattern and 1-D spectra, respectively. Patterns of ^{183}W NMR chemical shifts emerge from the homologous series. The structures of the hexametalate anions $[VW_5O_{19}]^{3-}$ and *cis*-$[V_2W_4O_{19}]^{4-}$ are also confirmed by ^{183}W NMR. Line-shape simulations of ^{183}W NMR resonances broadened by the quadrupolar ^{51}V are used to give the magnitude of the two bond couplings, $^2J_{W-O-V}$, and to demonstrate chemical exchange occurs. The two-bond coupling between vanadium and tungsten, $^2J_{W-O-V}$, parallels that between tungsten and tungsten, $^2J_{W-O-W}$, and allows assignment of resonances by inspection. Finally, connectivity patterns between adjacent inequivalent ^{51}V sites are detected by ^{51}V–^{51}V 2-D homonuclear correlation spectroscopy (COSY), providing information that is obscured in 1-D spectra.

Successful observation of tungsten-183 NMR spectra of polymetalates has provided an additional tool for structure determination in an area of chemistry traditionally beset with difficulty in species identification. Since the original work of Acerete, Hammer, and Baker was published,[1] the area has blossomed,[2-13] with most groups active in polymetalate chemistry using ^{183}W NMR data to supplement their research. By far the most widespread application is the use of simple integrated intensities of the ^{183}W lines to establish the solution symmetry. Typically, in these symmetrical species containing 6–30 tungsten atoms in the metal framework, the spectra consist of relatively few, well-resolved sharp lines. Because values of T_1 are 0.2–5 s, acquisition of spectra is feasible in periods of 1–10 h, in spite of the low receptivity of ^{183}W.

Lefebvre et al.[4] showed that the magnitude of the $^2J_{W-O-W}$ coupling constant, observable as ~7% satellites to the main lines, varied with W–O–W bond angle and provided a rational basis for distinguishing the mode of tungsten–tungsten atom connectivities in the metal atom backbone. Pairs of tungsten atoms sharing a common oxygen atom corner vertex have $^2J_{W-O-W}$ ~ 15–30 Hz while those edge-sharing a pair of oxygen atoms have $^2J_{W-O-W}$ ~ 5–12 Hz. It is important to establish W–O–W atom connectivities in these cyclic compounds because a complete assignment provides unequivocal proof of a structure. We have already applied these principles[7,8] to verify the structures of the Keggin anions $[PTiW_{11}O_{40}]^{5-}$ and 1,5-$[PTi_2W_{10}O_{40}]^{7-}$.

In more complex coupling problems the similarity of $^2J_{W-O-W}$ values can produce ambiguity in determination of connectivities. In principle, any ^{183}W can have up to 4 different adjacent ^{183}W atoms. Furthermore, the lower intensity of satellite lines makes them difficult to differentiate from major lines of slight impurities. These difficulties prompted Brevard et al.,[5a] and us,[8] to advocate 2-dimensional NMR (2-D) methods for establishing connectivity. The major advantage of the 2-D methods is that it is unnecessary to accurately measure the J value to establish the connectivity; the scalar coupling merely carries the chemical shift correlations for coupled sites, and differentiation is achieved on the basis of single- or double-quantum frequencies.

We apply and extend the above principles by presenting here detailed 1- and 2-dimensional ^{183}W NMR data to establish and substantiate the structures of several series of vanadium-substituted polytungstates. The compounds studied are the following: (i) monosubstituted Keggin anions ($[PVW_{11}O_{40}]^{4-}$, $[SiVW_{11}O_{40}]^{5-}$, and $[BVW_{11}O_{40}]^{6-}$); (ii) disubstituted Keggin anions (α-1,2-$[PV_2W_{10}O_{40}]^{5-}$ and α-1,2-$[SiV_2W_{10}O_{40}]^{6-}$); (iii) trisubstituted Keggin anions (α-1,2,3-$[PV_3W_9O_{40}]^{6-}$ and α-1,2,3-$[SiV_3W_9O_{40}]^{7-}$); and (iv) hexametalates ($[VW_5O_{19}]^{3-}$ and *cis*-$[V_2W_4O_{19}]^{4-}$).

The primary thrust of the investigation was the synthesis and identification of individual positional isomers[14] of higher substituted Keggin species and determination of chemical shift trends in a series of related compounds. We have noted earlier some trends in titanium(IV)-substituted anions,[7,8] and we were interested in the general effects of substitution of W(VI) by lower oxidation state metals.

The presence of vanadium(V) in the above structures substantially broadens the ^{183}W NMR lines of positions adjacent to the substitution site[3a] because of the quadrupolar properties of ^{51}V. Theoretical treatment of the observed line shapes and their temperature dependence is presented. Spectra recorded with decoupling of the interfering ^{51}V sharpen the ^{183}W resonances and allow connectivities to the determined from the scalar $^2J_{W-O-W}$ coupling via 1-D or 2-D methods.

Finally, we present novel 2-D ^{51}V–^{51}V connectivity data in the known anions $[V_{10}O_{28}]^{6-}$ and $[PV_{14}O_{42}]^{9-}$ which demonstrate that otherwise unattainable information can be derived from 2-D methods.

(1) Acerete, R.; Hammer, C. F.; Baker, L. C. W. *J. Am. Chem. Soc.* **1979**, *101*, 267–269.
(2) Acerete, R.; Harmalker, S.; Hammer, C. F.; Pope, M. T.; Baker, L. C. W. *J. Chem. Soc., Chem. Commun.* **1979**, 777–779.
(3) (a) Acerete, R.; Hammer, C. F.; Baker, L. C. W. *J. Am. Chem. Soc.* **1982**, *104*, 5384–5390. (b) Baker, L. C. W., private communication.
(4) LeFebvre, F.; Chauveau, F.; Doppelt, P.; Brevard, C. *J. Am. Chem. Soc.* **1981**, *103*, 4589–4591.
(5) (a) Brevard, C.; Schimpf, R.; Tourne, G.; Tourne, C. M. *J. Am. Chem. Soc.* **1983**, *105*, 7059–7063. (b) These experiments were carried out because original T_2 measurements, based on fitting a Lorentzian to the observed line shape ($T_2^{-1} = \pi\Delta\nu_{1/2}$), consistently showed $T_2 < T_1$. Later, precise T_2 measurements, using a Hahn spin-echo, showed the line-shape fitting was not valid because of contributions from ^{183}W isotopomer satellites. A single vanadium is surrounded by two pairs of tungsten atoms, so to first order the ^{51}V resonance is flanked by two pairs of 16% ^{183}W satellites with $^2J_{V-O-W}$ ~ 10 Hz and $^2J_{V-O-W}$ ~ 25 Hz. As a result, a natural line width of 22 Hz (T_2 = 14.5 ms) appears as a near Lorentzian with a measured line width of 30 Hz ("T_2" = 10.6 ms).
(6) Gansow, O. A.; Ho, R. K.; Klemperer, W. G. *J. Organomet. Chem.* **1980**, *187*, C27-31.
(7) Knoth, W. H.; Domaille, P. J.; Roe, D. C. *Inorg. Chem.* **1983**, *22*, 198–201.
(8) Domaille, P. J.; Knoth, W. H. *Inorg. Chem.* **1983**, *22*, 818–822.
(9) Finke, R. G.; Droege, M.; Hutchinson, J. R.; Gansow, O. A. *J. Am. Chem. Soc.* **1981**, *103*, 1587–1589.
(10) Finke, R. G.; Droege, M. *Inorg. Chem.* **1983**, *22*, 1006–1008.
(11) Sethuraman, P. R.; Leparulo, M. A.; Pope, M. T.; Zonnevijlle, F.; Brevard, C.; Lemerle, J. *J. Am. Chem. Soc.* **1981**, *103*, 7665–7666.
(12) Jeannin, Y.; Martin-Frere, J. *J. Am. Chem. Soc.* **1981**, *103*, 1664–1667.
(13) Kazansky, L. P.; Fedotov, M. A. *J. Chem. Soc., Chem. Commun.* **1983**, 417–419.
(14) Pope, M. T.; Scully, T. F. *Inorg. Chem.* **1975**, *14*, 953–954.

0002-7863/84/1506-7677$01.50/0

Experimental Section

Preparation of Compounds. Preparative procedures for all the monosubstituted Keggin anions ($[PVW_{11}O_{40}]^{4-}$, $[SiVW_{11}O_{40}]^{5-}$, $[BVW_{11}O_{40}]^{6-}$) and the hexametalates ($[VW_5O_{19}]^{3-}$, $[V_2W_4O_{19}]^{4-}$) have been reported in the literature,[15] but we give specific details of our methods since they are often slightly different, and the chemistry is sensitive to particular details. Because of the difficulty in obtaining reliable analyses, we favor spectroscopic identification (NMR) of compounds. Elemental analyses were performed by Galbraith or Pascher. Water content was determined by TGA.

α-$K_4[PVW_{11}O_{40}]$. (a) From $[PW_{11}O_{39}]^{7-}$ and VO_3^-. Fifty-four grams of $H_3PW_{12}O_{40}$ was dissolved in about 50 mL of water and solid Li_2CO_3 added slowly with vigorous stirring to bring the pH to 4.9. The solution was made up to a total volume of 75 mL, and 100 mL of 0.2 M $NaVO_3$ was added with stirring. HCl (6 M) was added dropwise to bring the mixture to pH 2 and the solution heated to 60 °C for 10 min before returning it to room temperature. Additional HCl was added to bring the mixture back to pH 2 and the solution reheated to 60 °C. Twenty grams of solid KCl was added and the solution maintained at 60 °C for a further 10 min. Cooling to 30 °C afforded a canary yellow solid which was collected by filtration (40 g).

Anal. (Galbraith) Calcd for $K_4[PVW_{11}O_{40}]\cdot 2H_2O$: K, 5.33; V, 1.73; P, 1.05; W, 68.87; H_2O, 1.23. Found: K, 5.06; V, 1.52; P, 1.03; W, 70.37; H_2O, 1.5.

NMR (^{31}P) −14.19 ppm; NMR (^{51}V) −557.3 ppm, $\Delta\nu_{1/2}$ = 26 Hz, pH 2.0, 30 °C.

(b) From $[PW_{11}O_{39}]^{7-}$ and VO^{2+}. Twenty-nine grams (10 mmol) of $H_3PW_{12}O_{40}$ was dissolved in 20 mL of water and approximately 2.6 g of solid Li_2CO_3 slowly added to bring the mixture to pH 4.8. A solution of 1.6 g of $VOSO_4$ in 5 mL of water was added dropwise over a period of 2 min to produce an ink black solution with final pH 1.9. Ten grams of KCl in 30 mL of water was added and the solution heated at 60 °C for 15 min. The volume of the solution was reduced to one-half the original and cooled to 0 °C to precipitate the product. Solid (7.8 g) was collected and dried. The volume of the filtrate was reduced again and cooled to crystallize a further 13.8 g of less-pure product. ^{31}P NMR of material oxidized with Br_2 shows the impurity to be unreacted $[PW_{11}O_{39}]^{7-}$. ^{31}P NMR of the oxidized form of the first crop shows it to be pure. Anal. (Pascher) Calcd for $K_5[PV^{IV}W_{11}O_{40}]\cdot 8H_2O$: K, 6.34; P, 1.00; V, 1.65; W, 65.6; H_2O, 4.7. Found: K, 6.58; P, 1.02; V, 1.55; W, 66.0; H_2O, 4.6.

The more soluble lithium salt was obtained from 5 g of $K_4[PVW_{11}O_{40}]$ dissolved in a minimum of water and passed through 5 g of Rexyn 101 which had been converted to the lithium form. The eluted solution was stripped to dryness to give 3.5 g of product.

α-$K_5[SiVW_{11}O_{40}]$. (a) From $[SiW_{11}O_{39}]^{8-}$ and VO_3^-. $H_4SiW_{12}O_{40}$ (41.4 g, 14.5 mmol) was dissolved in 25 mL of H_2O with heating to 80 °C. Approximately 13.8 g of $NaHCO_3$ was added and the solution cooled to room temperature and filtered (pH 8.2). ^{183}W NMR shows a clean spectrum of $[SiW_{11}O_{39}]^{8-}$. $NaVO_3$ (4.9 g, 40 mmol) was stirred in and 6 M HCl added dropwise with continued boiling for 1 min. The cooled solution (pH 5.5) was filtered to remove V_2O_5 which had formed. The solution was reheated to 80 °C and 6.5 g of KCl added. A yellow precipitate was collected after the mixture was cooled to room temperature. The product was recrystallized from 20 mL of 80 °C water at pH 6 after the mixture was cooled in an ice bath. Product (14.3 g) was collected. A second crop yielded a further 4.6 g. Further recrystallization of the combined products gave a final yield of 13.5 g.

The potassium salt was not analyzed but immediately converted to the lithium form by stirring the mixture overnight with 20 g of Rexyn 101 (Li^+) and passing the complete mixture through a further 20 g of ion-exchange resin in a column. The stripped product (12 g) was used for ^{183}W NMR studies.

Anal. (Pascher) Calcd for $Li_5[SiVW_{11}O_{40}]\cdot 8H_2O$: Li, 1.19; Si, 0.96; V, 1.74; W, 69.3; H_2O, 4.9. Found: Li, 1.19; Si, 0.95; V, 1.85; W, 68.1; H_2O 5.1. NMR (^{29}Si) −84.84 ppm; NMR (^{51}V) −550.8 ppm, $\Delta\nu_{1/2}$ = 33 Hz, 30 °C, pH 2.

Repeat syntheses have shown the above method is difficult to reproduce and method b provides greater reliability.

(b) From $[SiW_{11}O_{39}]^{8-}$ and VO^{2+}. $H_4SiW_{12}O_{40}$ (28.8 g, 10 mmol) was dissolved in 25 mL of water with warming to 40 °C. Slowly, 7.2 g of solid $NaHCO_3$ was added to raise the pH to 7.9. A solution of 3 g (18 mmol) of $VOSO_4$ in 5 mL of water was added dropwise and then the solution heated for 30 min at 60 °C. Solid KCl (10 g) was slowly added and the temperature maintained at 60 °C for a further 15 min. The solution was cooled to 0 °C for 15 min and 23 g of black crystalline material collected by filtration. The product was recrystallized once from 80 to 0 °C to give 19.4 g of finely crystalline material. ^{51}V NMR of the oxidized form (Br_2) shows clean product.

Anal. (Pascher) Calcd for $K_6[SiV^{IV}W_{11}O_{40}]\cdot 2H_2O$: K, 7.79; V, 1.69; W, 67.1; H_2O, 1.2. Found: K, 7.29; V, 1.71; W, 66.2; H_2O, 1.1.

α-$K_6[BVW_{11}O_{40}]$. $Na_2WO_4\cdot 2H_2O$ (36.3 g, 0.11 mol) was dissolved in a total volume of 75 mL of water with gentle warming. The solution was returned to room temperature and glacial CH_3COOH added dropwise to bring the pH from 9.4 to 6.3. Total volume is approximately 90 mL. H_3BO_3 (2.47 g, 0.04 mol) was slowly added with stirring. Some undissolved solid remained until the solution was heated to 80 °C whereupon it clarified. $VOSO_4$ (1.8 g) in 3 mL of water was added dropwise to produce a dark blue-black solution. Solid KCl (20 g) was added slowly and after being stirred for 5 min at 80 °C, the solution was cooled to 0 °C for 30 min. The precipitate was collected and the filtrate discarded. All the precipitate was added to 60 mL of water and a few drops of CH_3COOH added to reduce the pH to 5. The solution was heated to 90 °C and filtered hot to leave a light purple solid. The filtrate was reheated to boiling and allowed to cool overnight on a warm hot plate to produce 15–20 g of black long needlelike crystals. All but 0.5 g of product was slurried in 50 mL of water and warmed to 50 °C. Neat Br_2 liquid was added until a lemon yellow solution resulted. The solution was filtered hot to leave a white crystalline material, and the filtrate volume was reduced to 15–20 mL before being cooled to 0 °C. Yellow crystals (12–15 g) were collected. Anal. (Pascher) Calcd for $K_6[BVW_{11}O_{40}]\cdot 3H_2O$: K, 7.79; B, 0.36; V, 1.69; W, 67.1; H_2O, 1.8. Found: K, 7.52; B, 0.35; V, 1.66; W, 66.2; H_2O, 1.6.

NMR (^{51}V) −576.4 ppm; $\Delta\nu_{1/2}$ = 16 Hz, 30 °C, pH 2.0.

All the potassium salt was slurried in 25 mL of water at room temperature and 20 g of Rexyn 101 (Li^+) added with continued stirring for 3 h. The solution was isolated by filtration and stripped to dryness. The compound was warmed gently with 10 mL of D_2O with stirring and reduced to a total volume of 7 mL for ^{183}W NMR.

α-1,2,3-$K_6H[SiV_3W_9O_{40}]$ and α-1,2-$K_6[SiV_2W_{10}O_{40}]$. Both of these compounds were isolated with varying yields from the same preparative procedures involving either $NaVO_3$ or $VOSO_4$. The following is typical of several efforts:

$NaVO_3$ (5.5 g, 45 mmol) and 40 g of α-$Na_{10}[SiW_9O_{34}]$[16] (15 mmol) were mixed as dry powders and added to 400 mL of water at room temperature. The solution was stirred vigorously and 6 M HCl added dropwise to bring the pH to 1.5, and a clear wine red solution developed.[17] Solid KCl (50 g) was stirred into the solution to leave a clear solution. Methanol (1.5 L) was then added and the solution left to sit 60 h after which time the orange precipitate was collected. The solid was dissolved in water at 65 °C and filtered, and the filtrate was cooled to 0 °C to form 2.3 g of an orange brown powder later identified as α-1,2,3-K_6H-$[SiV_3W_9O_{40}]$.

Anal. (Pascher) Calcd for $K_6H[SiV_3W_9O_{40}]\cdot 3H_2O$: K, 8.48; Si, 1.02; V, 5.53; W, 59.84; H_2O, 2.0. Found: K, 8.24; Si, 1.01; V, 5.50; W, 59.3; H_2O, 2.0.

NMR (^{29}Si) −84.38 ppm; NMR (^{51}V) −573.1, $\Delta\nu_{1/2}$ = 320 Hz, 30 °C, pH 1.5.

The remaining filtrate was reduced in volume to produce further crops of 1.3 and 1.1 g containing successively more $K_6[SiV_2W_{10}O_{40}]$. Finally, the filtrate was stripped to dryness to give 14.0 g of a light orange powder. This material was washed with 20 mL of 40 °C water to leave 3.6 g of solid. The filtrate was cooled to 0 °C to give 3.9 g of orange crystals. These crystals were taken up in 8 mL of water and cooled slowly to room temperature to yield 1.8 g of large dark red crystals which were considered analytically pure α-1,2-$K_6[SiV_2W_{10}O_{40}]$.

Anal. (Pascher) Calcd for α-1,2-$K_6[SiV_2W_{10}O_{40}]\cdot 4.5H_2O$: K, 8.03; Si, 0.96; V, 3.48; W, 62.9; H_2O, 2.5. Found: K, 8.03; Si, 0.94; V, 3.38; W, 62.2; H_2O, 2.6.

NMR (^{29}Si) −84.28 ppm; NMR (^{51}V) −550.2 ppm, $\Delta\nu_{1/2}$ = 116 Hz, 30 °C, pH 1.5.

Less pure samples were used for ^{183}W NMR in the interest of maximizing sensitivity.

α-1,2-$K_5[PV_2W_{10}O_{40}]$. $Na_8H[PW_9O_{34}]$[18] (30 g, 12.5 mmol) was added to 60 mL of vigorously stirred 20 °C water to produce a white slurry. After 1 min a solution of 4.2 g of $VOSO_4$ (26 mmol) in 17 mL of water was added dropwise over a period of 10 min and the reaction mixture stirred for an additional 30 min at 20 °C. The temperature of the

(15) (a) $[PVW_{11}O_{40}]^{4-}$: Smith, D. P.; So, H.; Bender, J.; Pope, M. T. *Inorg. Chem.* **1973**, *12*, 685–688. (b) $[SiVW_{11}O_{40}]^{5-}$: ref 3, 15c. (c) $[BVW_{11}O_{40}]^{6-}$: Altenau, J. J.; Pope, M. T.; Prados, R. A.; So, H. *Inorg. Chem.* **1975**, *14*, 417–421. (d) $[VW_5O_{19}]^{3-}$, $[V_2W_9O_{19}]^{4-}$: Flynn, C. M.; Pope, M. T. *Inorg. Chem.* **1971**, *10*, 2524–2529.

(16) Herve, G.; Teze, A. *Inorg. Chem.* **1977**, *16*, 2115–2117.

(17) This procedure was based upon unpublished work of R. G. Finke and B. Rapko for the analogous β-$Na_9H[SiW_9O_{34}]$ starting material.

(18) Massart, R.; Contant, R.; Fruchart, J. M.; Ciabrini, J. P. *Inorg. Chem.* **1977**, *16*, 2916–2921.

mixture was increased to 60 °C for 1 h and then Br_2 added until a clear orange solution resulted. Solid KCl (25 g) was stirred in and the mixture heated briefly to 80 °C and then filtered while hot. The cooled filtrate produced 28.3 g of crystalline orange product which ^{31}P NMR showed to be 85% of the 1,2-positional isomer.[19] Recrystallization from 80 °C, pH 2 water gave analytically pure material. A 5×10^{-3} M solution in 0.5 M KCl/HCl at pH 2 maintained at 80 °C for 16 h shows minimal rearrangement to other positional isomers.

Anal. (Pascher) Calcd for $K_5[PV_2W_{10}O_{40}]\cdot 3H_2O$: K, 6.83; P, 1.08; V, 3.56; W, 64.3; H_2O, 1.8. Found: K, 6.83; P, 1.07; V, 3.48; W, 63.6; H_2O, 1.8.

NMR (^{31}P) −13.61 ppm; NMR (^{51}V) −548.6 ppm, $\Delta\nu_{1/2}$ = 122 Hz, pH 2.0, 30 °C.

α-1,2,3-$K_6[PV_3W_9O_{40}]$. $NaVO_3$ (6.1 g, 50 mmol) was added to 200 mL of 1.0 M sodium acetate/acetic acid buffered at pH 4.8. $Na_8H[PW_9O_{34}]$ (40 g, 15 mmol) was added and the solution stirred at 25 °C for 48 h. The solution was then divided into two equal portions. The first was treated with 15 g of solid KCl and stirred for 30 min. Methanol (250 mL) was added to produce precipitate which was filtered to give 22 g of tan-orange powder.

Anal. (Pascher) Calcd for $K_6[PV_3W_9O_{40}]\cdot 4H_2O$: K, 8.42; P, 1.11; V, 5.49; W, 59.4; H_2O, 2.6. Found: K, 8.10; P, 1.09; V, 5.45; W, 59.3; H_2O, 2.9.

NMR (^{31}P) −13.41 ppm, pH 1.8; NMR (^{51}V) −566.1 ppm, $\Delta\nu_{1/2}$ = 275 Hz, pH 1.8, 30 °C.

The remaining portion was treated dropwise with a saturated solution of CsCl until no further precipitation occurred. The product was filtered and washed with 2 × 100 mL of 25 °C water. Attempts to recrystallize the product from 80 °C water produced isomerization. Subsequent preparations were not recrystallized.

Anal. (Galbraith) Calcd for $Cs_6[PV_3W_9O_{40}]$: Cs, 24.32; V, 4.67; W, 50.04; P, 1.01. Found: Cs, 24.05; V, 4.36; W, 49.07; P, 0.91.

The quite insoluble yellow cesium salt was slurried with 500 mL of water and added to a column of 100 g of lithium ion exchange resin (Rexyn 101). At the slurry/resin interface, a wine red solution formed which eluted cleanly. The solution was stripped to dryness at room temperature. ^{31}P, ^{51}V, and ^{183}W NMR showed clean product.

$[(n\text{-}C_4H_9)_4N]_3[VW_5O_{19}]$. $Na_2WO_4\cdot 2H_2O$ (13.2 g, 40 mmol) and $NaVO_3$ (1 g, 8.2 mmol) were dissolved in 1800 mL of water and heated to 80 °C for 5 min. H_2SO_4 (80 mL, 0.5 M) was slowly added and the mixture maintained at 80 °C for 20 min. A saturated aqueous solution of 10 g of $(n\text{-}C_4H_9)_4NBr$ (TBABr) was added and the solution cooled slowly to room temperature on the hot plate. The precipitate was collected and washed with water before recrystallization from boiling acetonitrile. Yield 15.6 g.

Anal. (Pascher) Calcd for $[(nC_4H_9)_4N]_3[VW_5O_{19}]$: C, 28.80; H, 5.44; N, 2.10; V, 2.55; W, 45.9. Found: C, 28.65; H, 5.46; N, 2.22; V, 2.54; W, 45.8.

NMR (^{51}V) −509.6, $\Delta\nu_{1/2}$ = 5 Hz, 30 °C, CD_3CN.

***cis*-$Li_4[V_2W_4O_{19}]$.** $NaVO_3$ (3.65 g, 30 mmol) and $Na_2WO_4\cdot 2H_2O$ (19.8 g, 60 mmol) were dissolved in 150 mL of water by heating the mixture to boiling for 2 min. The solution was then cooled to 60 °C and 3 M HCl added dropwise to bring the pH to 3.0. The solution was briefly reheated to boiling and returned to 25 °C. A saturated solution of 12 g of CsCl in water was added to form a yellow-orange precipitate. The solid was collected and recrystallized from boiling water. Initial solids contained $[V_{10}O_{28}]^{6-}$, but the filtrate showed pure $[V_2W_4O_{19}]^{4-}$ (^{51}V NMR). This solution was passed through a column of Rexyn 101 (Li^+) and the resultant solution stripped to dryness. Yield 4.3 g.

Anal. (Pascher) Calcd for $Li_4[V_2W_4O_{19}]\cdot H_2O$: Li, 2.34; V, 8.58; W, 62.0; H_2O, 1.5. Found: Li, 1.98; V, 8.36; W, 57.8; H_2O, 1.7.

NMR (^{51}V) −510.5 ppm, $\Delta\nu_{1/2}$ = 18 Hz, 30 °C, pH 5.5; NMR (^{31}V) −523.2 ppm, $\Delta\nu_{1/2}$ = 31 Hz, pH 2, 30 °C.

$[PV_{14}O_{42}]^{9-}$. $NaVO_3$ (2.44 g, 20 mmol) was added to 20 mL of 80 °C water. H_3PO_4 (3.4 mL, 1.5 M, 3.8 mmol) was added with stirring, the solution cooled to room temperature, and 3 M HNO_3 added to bring the pH to 2.4. ^{51}V NMR showed the desired product[20] with a major impurity of $[V_{10}O_{28}]^{6-}$. More HNO_3 was added to bring the solution to a final pH of 1.7 where ^{51}V NMR showed clean product. The compound was not isolated and the solution used for 2-D ^{51}V NMR.

NMR (^{51}V) −528.1 (2,230 Hz), −580.0 (8,350 Hz), −593.8 ppm (4,470 Hz); 60 °C, pH 1.7.

$[V_{10}O_{28}]^{6-}$. $NaVO_3$ was dissolved in 5 mL of water and 4 M HCl added to bring the pH to 4.8. Additional $NaVO_3$ was added whenever the solution became clear and additional HCl added to maintain pH 4.8. The solution was filtered and reduced to pH 4.5 with additional HCl, and the identity of $V_{10}O_{28}^{6-}$ was established by ^{51}V NMR.[21] Product was not isolated but the solution used directly for 2-D ^{51}V NMR.

NMR (^{51}V) −421 (2,230 Hz), −497 (4,160 Hz), −513 ppm (4,110 Hz).

NMR Measurements. All NMR data were obtained with a Nicolet NT-360WB spectrometer utilizing a NIC-1280 computer and 293B pulse programmer.

^{183}W NMR spectra (15 MHz) were recorded either in a 20 mm diameter sideways spinning solenoidal probe[22] ($\pi/2$ pulse 50–80 μs) or in a vertical 20 mm diameter Helmholtz coil probe ($\pi/2$ pulse 200–500 μs). The solenoidal probe is restricted in temperature range to 10–40 °C but provides superior H_1 pulse homogeneity necessary for 2-dimensional pulse sequences and T_1 measurements. It is also equipped with a concentric tunable decoupler coil (50–150 MHz). The vertical probe is used for variable-temperature studies of both 12 mm and 20 mm diameter samples where high H_1 pulse homogeneity and ^{51}V decoupling are not needed.

^{51}V decoupling is achieved by intercepting a software controlled synthesizer signal (94 MHz) and directing it to an Amplifier Research 10LA amplifier. The output power (0.1–4 W) is directed through a band-pass filter to the tuned decoupler coil. The tuned circuit is not especially efficient ($Q \sim 35$) since the design sacrifices quality factor for large range frequency tunability. The broad-band preamplifier of the receiver channel was protected from decoupler overload by insertion of an in-line 15-MHz band-pass filter (Cir-Q-Tel).

^{183}W NMR are recorded in appropriate perdeuterated solvents (normally D_2O for alkali metal salts) and referenced to external 2 M Na_2WO_4 in D_2O at 30 °C. Shifts are thus sensitive to induced shifts in the solvent.

^{31}P, ^{51}V, and ^{29}Si NMR spectra are obtained in a conventional 12 mm diameter broad-band probe with use of a nondeuterated solvent with a concentric D_2O capillary for field frequency lock. Spectra are externally referenced to 85% H_3PO_4, neat $VOCl_3$, and Me_4Si at 30 °C for ^{31}P, ^{51}V, and ^{29}Si, respectively. Spectra recorded in this manner are not sensitive to solvent shifts induced by pH, exchange, etc. Over a period of 2 years ^{31}P chemical shifts have remained consistent to 0.02–0.05 ppm in spite of slightly different conditions due to a slowly drifting magnet. Chemical shifts to low frequency of the reference are negative.

T_1 measurements (^{183}W, ^{51}V) were accomplished with the inversion recovery sequence with use of a composite π-pulse[23] (−recycle decay−$\pi/2(x)\pi(y)\pi/2(x)-\tau-\pi/2(x)$−acquire−). Intensities were measured by integration where possible and from interpolated peak heights in cases of near overlap. Intensity vs. time data were directly fit by using a three-parameter function[24] from standard Nicolet software.

2-Dimensional (2-D) ^{183}W–^{183}W connectivity experiments were done with the 2-D INADEQUATE sequence[25] with the Mareci–Freeman modification[26] of a $3\pi/4$ conversion pulse and 128-step phase cycling. The complete sequence can be written (−recycle time−$\pi/2(x)$−$D(3)$−$\pi/2(A)\pi(A+1)\pi/2(A)$−$D(3)$−$\pi/2(B)$−t_1−$3\pi/4(C)$−acquire(D)−) where A, $A+1$, B, C, and D represent the phase cycling of the radio-frequency pulses and receiver: $D(3)$ was set to 40 ms to optimize conversion into

A: $(x)*32\,(y)*32\,(-x)*32\,(-y)*32$
$A+1$: $(y)*32\,(-x)*32\,(-y)*32\,(x)*32$
B: $((x)*16\,(-x)*16)*4$
C: $((x)*4\,(y)*4\,(-x)*4\,(-y)*4)*8$
D: $\{(x)*4\,(-y)*4\,(-x)*4\,(y)*4\,(-x)*4\,(y)*4\,(x)*4\,(-y)*4$ / $(-x)*4\,(y)*4\,(x)*4\,(-y)*4\,(x)*4\,(-y)*4\,(-x)*4\,(y)*4\}*2$

double quantum coherence, $D(3) = (2n+1)/4J_{W\text{-}O\text{-}W}$ for $J \sim 6$ Hz ($n = 0$) and $J \sim 19$ Hz ($n = 1$). The transmitter was placed in the center of the two extreme chemical shifts and t_1 incremented by the maximum computer dwell time which allowed faithful detection of all double quantum frequencies. For optimum efficiency the number of data files collected (t_1 increments) were determined from the digital resolution necessary to distinguish all possible frequencies in the double quantum dimension; typically 16–128 files were collected. The time of the ex-

(19) Later preparations in which the reaction was run for extended periods at 25 °C gave higher specificity to the α-1,2 isomer (>95%) but increased amounts of $K_4[PVW_{11}O_{40}]$. The latter could be removed by crystallization, but a lower overall yield (7 g) of the α-1,2 isomer results.

(20) Kato, R.; Kobayashi, A.; Sasaki, Y. *Inorg. Chem.* **1982**, *21*, 240–246.

(21) O'Donnell, S. E.; Pope, M. T. *J. Chem. Soc. Dalton Trans.* **1976**, 2290–2297.

(22) Similar in design to that described by Bailey et al.: Bailey, J. T.; Rosanske, R. C.; Levy, G. C. *Rev. Sci. Instrum.* **1981**, *52*, 548–552.

(23) Cutnell, J. D.; Bleich, H. E.; Glasel, J. A. *J. Magn. Reson.* **1976**, *21*, 43. Freeman, R.; Kempsell, S. P.; Levitt, M. H. *J. Magn. Reson.* **1980**, *38*, 453–479.

(24) Levy, G.; Peat, I. *J. Magn. Reson.* **1975**, *18*, 500.

(25) (a) Bax, A. "Two dimensional Nuclear Magnetic Resonance in Liquids"; Delft University Press: Delft, 1982. (b) Bax, A.; Freeman, R.; Kempsell, S. P. *J. Am. Chem. Soc.* **1980**, *102*, 4849–4851.

(26) Mareci, T. H.; Freeman, R. *J. Magn. Reson.* **1982**, *48*, 158–163.

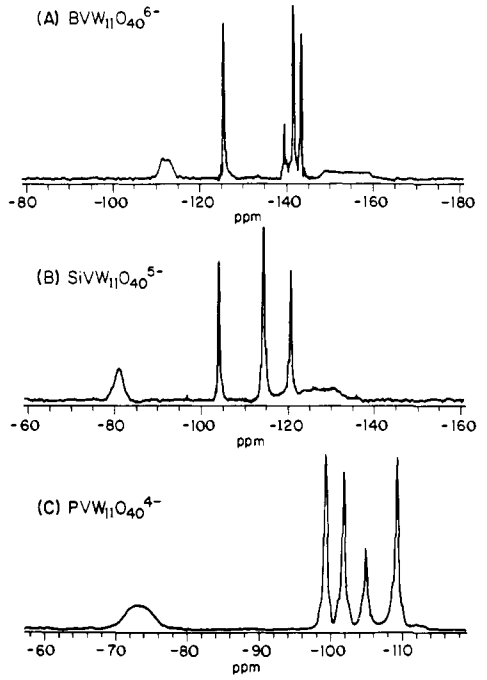

Figure 1. Conventional 1-D ^{183}W NMR spectra of $Li_6[BVW_{11}O_{40}]$, $Li_5[SiVW_{11}O_{40}]$, and $Li_4[PVW_{11}O_{40}]$: (A) 5 mL of 0.6 M $Li_6[BVW_{11}O_{40}]$ in D_2O, 40 °C, 40 000 transients, 2.85 h, 12-mm vertical tube, LB = 2.5 Hz; (B) 5 mL of 0.6 M $Li_5[SiVW_{11}O_{40}]$ in D_2O, 40 °C, 32 000 transients, 2.3 h, 12-mm vertical tube, LB = 2.0 Hz; (C) 5 mL of 0.6 M $Li_4[PVW_{11}O_{40}]$ in D_2O, 25 °C, 16 384 transients, 2.3 h, 20-mm sideways tube, LB = 2.0 Hz.

periment is directly related to this requirement of digital resolution. For the modest number of distinct sites it is a simple task to compute all the feasible double quantum frequencies prior to the 2-D experiment and decide upon the number of files necessary. Free induction decay data were processed with apodization by exponential multiplication in the first dimension (F_2). No apodization was used in the second (F_1) dimension. Data are displayed as 3-dimensional contour plots or by retrieving specific rows of the data matrix.

2-Dimensional ^{51}V–^{51}V connectivity data were obtained by using the well-known COSY90 sequence[27] (-recycle delay-$\pi/2(A)$-t_1-$\pi/2(B)$-acquire-) where

$$A\text{: } (x)^*4\,(y)^*4\,(-x)^*4\,(-y)^*4$$

$$B\text{: } (x)(y)(-x)(-y)$$

t_1 was incremented by the dwell time, and typically 256 × 512 word files were acquired. Data were apodized in both dimensions by a cosine-bell function, i.e., $\sin^2(j\pi/N)$ where $j = 0$ to $N - 1$ for an N-point FID.

Specific details of number of scans, apodization parameters, and solution concentration are given in the text where appropriate.

Results

(a) 1-D ^{183}W NMR of Monosubstituted Keggin Anions. The ^{183}W NMR spectra of $[PVW_{11}O_{40}]^{4-}$, $[SiVW_{11}O_{40}]^{5-}$, and $[BVW_{11}O_{40}]^{6-}$ are shown in Figures 1 and 2. ^{51}V decoupling (Figure 2) sharpens the lines of those tungsten sites adjacent to the quadrupolar ^{51}V ($S = {}^7/_2$) and reveals six resonances[28] of relative intensity 2:2:2:2:2:1, consistent with a C_s monosubstituted α-Keggin structure. However, the measured intensity ratios are a necessary, but insufficient, criterion to unambiguously establish the α-arrangement; β_1-$[XVW_{11}]$, β_3-$[XVW_{11}]$, and selected isomers of the Baker–Figgis γ, δ, and ϵ forms are also feasible, although unlikely, C_s structures. Detailed connectivity arguments which unambiguously establish the α-configuration are presented later.

In the coupled spectra (Figure 1) the highest frequency tungsten resonance is from a site adjacent to ^{51}V, and some broadening of the line results. More substantial broadening occurs in the lowest frequency lines of $[SiVW_{11}O_{40}]^{5-}$ and $[BVW_{11}O_{40}]^{6-}$ and

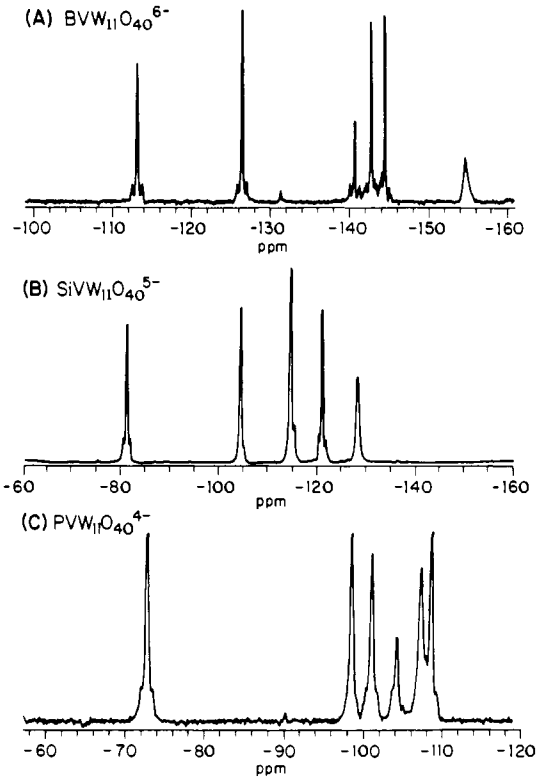

Figure 2. ^{51}V decoupled 1-D ^{183}W NMR spectra: (A) $Li_6[BVW_{11}O_{40}]$, 0.6 M, 30 °C, 1024 transients, 0.7 h, 1-W ^{51}V decoupling, 20-mm sideways tube, LB = 1.0 Hz; (B) $Li_5[SiVW_{11}O_{40}]$, 0.6 M, 30 °C, 20 000 transients, 15.2 h, 2-W ^{51}V decoupling, 20-mm sideways tube, LB = 1.0 Hz; (C) $Li_4[PVW_{11}O_{40}]$, 0.6 M, 30 °C, 8000 transients, 1.1 h, 3-W ^{51}V decoupling, 20-mm sideways tube, LB = 1.0 Hz.

in the next to lowest frequency resonance in $[PVW_{11}O_{40}]^{4-}$. Clearly these different line shapes depend on the mode of attachment of vanadium to tungsten; different $^2J_{W\text{-}O\text{-}V}$ values are anticipated for edge- and corner-coupled sites. Baker and coworkers,[3a] using a 90-MHz spectrometer, were unsuccessful in observing tungsten sites adjacent to ^{51}V, and they presented an estimate of the broadening ($T_2(^{183}W)$) due to scalar relaxation of the second kind. Although this treatment is valid for estimating the *line width* of the ^{183}W in the presence of rapid relaxation of ^{51}V, it does not provide information on the *line shape* in the intermediate relaxation regime. Below we show how accurate fitting of the line shape can be used to measure the magnitude of the two-bond vanadium–tungsten scalar coupling, $^2J_{W\text{-}O\text{-}V}$.

Line-shape theory of an $I = {}^1/_2$ nucleus scalar coupled to a quadrupolar nucleus S undergoing relaxation is well documented in the literature.[29] In the simplest case, the line shape depends on the spin–lattice relaxation time of the quadrupolar nucleus, T_{1q}, and the magnitude of the scalar coupling of the I, S spin system, $J_{IS}\mathbf{I}\cdot\mathbf{S}$. If the relaxation rate of the S spin is slow relative to J_{IS} ($\tau \ll J_{IS}$), the I spin will see $(2S + 1)$ equally populated sites and the spectrum of the I spin will consist of $(2S + 1)$ lines of equal intensity. As the S spin undergoes more rapid relaxation ($\tau \sim J_{IS}$), the I spin spectrum broadens with a characteristic line shape. When S relaxation occurs at a rate $\tau \gg J_{IS}$ the I and S spins are effectively decoupled from each other and a single line results in the spectrum of the I spin. Naturally, the quantitative line shape depends on the mechanism of S-spin relaxation. Quadrupolar relaxation is governed by the selection rule $\Delta m_S = \pm 1, \pm 2$ whereas chemical exchange is nonselective as far as changes in m_S are concerned. Most previous work on other spin systems has neglected chemical exchange and independently varied T_{1q} and J_{IS} to provide the best visual match of the computed line shape with experiment. We are able to independently measure

(27) Bax, A.; Freeman, R.; Morris, G. *J. Magn. Reson.* **1981**, *42*, 164.
(28) In $[SiVW_{11}O_{40}]^{5-}$ two lines of intensity 2 and 1 overlap at −114.6 ppm.
(29) See, for example: Aksnes, D. W.; Hutchison, S. M.; Packer, K. J. *Mol. Phys.* **1968**, *14*, 301–309 and references therein.

Table I. T_1 Measurements of ^{51}V in the Series of Anions $XVW_{11}O_{40}^{n-}$ (X = B, Si, P; n = 6, 5, 4) and $^2J_{V\text{-}O\text{-}W}$ from Simulation of ^{183}W Line Shapes[a]

	T_1, ms		
temp, °C	$BVW_{11}O_{40}^{6-}$	$SiVW_{11}O_{40}^{5-}$	$PVW_{11}O_{40}^{4-}$
20	9.4	2.9	4.2
40	13.8	4.3	
60	19.9	6.7	8.0
80	26.3	9.6	11.4
100	33.1	11.8	
$^2J_{V\text{-}O\text{-}W}$(edge)	9 ± 1	11.5 ± 1	15.5 ± 1
$^2J_{V\text{-}O\text{-}W}$(corner)	26 ± 2	25 ± 5	25 ± 5

[a] Relaxation measurements were performed on saturated 25 °C solutions of the appropriate lithium salts, typically 0.6–0.8 M. These same solutions were used for variable-temperature ^{183}W NMR line-shape studies.

the T_1 values of ^{51}V in our heteropolyanions and use more complete theory to extract the magnitudes of $^2J_{V\text{-}O\text{-}W}$ in these compounds. Line-shape simulations are carried out and compared with experimental determinations at different temperatures.

(b) Line-Shape Theory. The intensity of the NMR absorption of the I spins is described by the equation[30]

$$I(\omega) \propto \mathrm{Re}\{\mathbf{W}\cdot\mathbf{A}^{-1}\cdot\mathbf{1}\} \quad (1)$$

where **W** is a row vector whose components are proportional to the relative populations of the $(2S + 1)$ spin states of S (all unity in the high-temperature limit) and **1** is a unit column vector. $\mathbf{A}^{-1}$ is the $(2S + 1) \times (2S + 1)$ inverse of the matrix **A** with elements given by the expression

$$A_{mm'} = [i(\omega_0 - \omega + 2\pi Jm) - \tau_m^{-1}]\delta_{mm'} + P_{mm'} \quad (2)$$

ω_0 is the center of the I multiplet; $P_{mm'}$ is the probability per unit time of transitions between states m and m' of the S spin; $\delta_{mm'}$ is the delta function; and τ_m is the average lifetime of the state m of spin S as the sum of all transition probabilities.

$$\tau_m^{-1} = \sum_{m'} P_{m,m'} \quad (3)$$

Quadrupolar transitions are restricted to m changes of 1 or 2 with the following matrix elements

$$R_{m,m\pm1} = \frac{(2m \pm 1)^2(S \pm m + 1)(S \mp m)}{2(2S - 1)(2S + 3)}(T_{1q})^{-1} \quad (4a)$$

$$R_{m,m\pm2} = \frac{(S \mp m)(S \mp m - 1)(S \pm m + 1)(S \pm m + 2)}{2(2S - 1)(2S + 3)}(T_{1q})^{-1} \quad (4b)$$

T_{1q} is the quadrupolar contribution to T_1. If only quadrupolar relaxation is important, $P_{m,m'} = R_{m,m'}$.

If chemical exchange, characterized by a lifetime τ_{ex}, also occurs the lifetime of the S states is reduced because of an extra term

$$\tau_m^{-1} = \sum_{m'} R_{m,m'} + \tau_{ex}^{-1} \quad (5a)$$

and

$$P_{m,m'} = R_{m,m'} + (1/2S)\tau_{ex}^{-1} \qquad (m \neq m') \quad (5b)$$

The m selectivity of quadrupolar relaxation causes more rapid broadening of the inner lines while the outer pair remain sharper; the relative lifetimes are $^5/_{14}{:}^5/_{26}{:}^5/_{24}{:}^5/_{20}$ for $m = \pm^7/_2, \pm^5/_2, \pm^3/_2, \pm^1/_2$, respectively. On the other hand, chemical exchange is not m dependent and equally broadens all multiplet components. In this sense, any non-m-selective relaxation mechanism of S will be manifested as "chemical exchange".

(c) ^{51}V T_1 Measurements and ^{183}W NMR Line Shapes. Table I contains measurements of T_1 (^{51}V) of the monosubstituted heteropolyanions as a function of temperature. These same solutions were used to obtain the ^{183}W NMR spectra for line-shape analysis. Within experimental error, $T_1 = T_2$ indicating that quadrupolar relaxation is dominant. Both relaxation times are observed to be independent of polyanion concentration (except for viscosity effects), pH, added VO_2^+, and magnetic field strength.[5b]

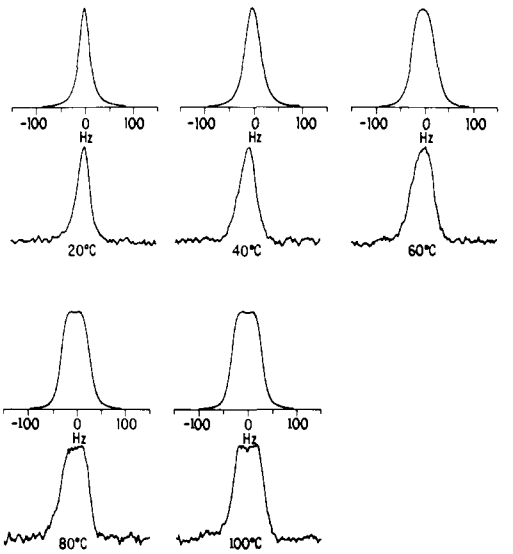

Figure 3. Observed and calculated line shape of −81.1 ppm ^{183}W NMR resonance of 0.6 M $Li_5[SiVW_{11}O_{40}]$ as a function of temperature. Simulations are with $^2J_{W\text{-}O\text{-}V}$ = 11.5 Hz, $\tau_{ex} = 40\ s^{-1}$, and $T_1(^{51}V)$ values in Table I.

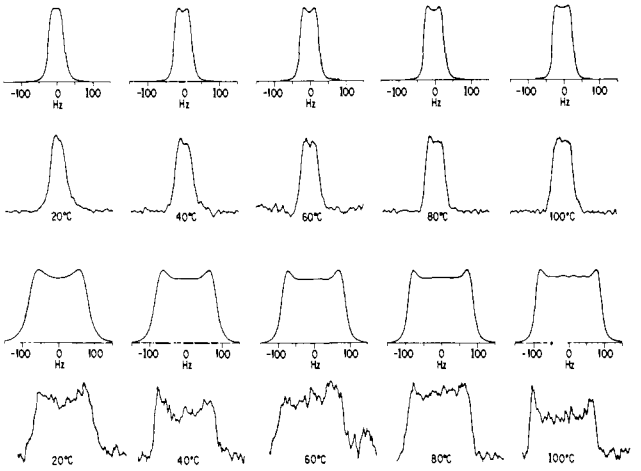

Figure 4. Observed and calculated line shapes of −113.2 ppm (upper) and −154.8 ppm (lower) ^{183}W NMR resonances of 0.6 M $Li_6[BVW_{11}O_{40}]$ as a function of temperature. Simulations are with $^2J_{W\text{-}O\text{-}V}$ = 9 Hz (upper), $^2J_{W\text{-}O\text{-}V}$ = 26 Hz (lower), $\tau_{ex} = 20\ s^{-1}$, and $T_1(^{51}V)$ values in Table I.

Figure 3 shows the observed and calculated line-shapes of the highest frequency line of $[SiVW_{11}O_{40}]^{5-}$ when the measured T_1 (^{51}V) values are used. Significantly worse fits are obtained if chemical exchange is not included although it is difficult to define an accurate value of τ_{ex}. The line shapes are best fit with a constant $\tau_{ex} \sim 20$–$50\ s^{-1}$ over the whole temperature range and $^2J_{W\text{-}O\text{-}V}$ = 11.5 ± 1 Hz. The low-frequency resonance is fit with the same τ_{ex} and $^2J_{W\text{-}O\text{-}V}$ = 25 ± 5 Hz but is not shown because of overlap with an uncoupled ^{183}W site.

Figure 4 shows the line shape of both the high- and low-frequency resonances of $[BVW_{11}O_{40}]^{6-}$. Good fits are obtained with $^2J_{W\text{-}O\text{-}V}$ = 9 and 26 Hz, respectively, and $\tau_{ex} \sim 20\ s^{-1}$. Subsequently, we have observed ^{183}W satellite structure in the sharp ^{51}V NMR spectrum of a dilute solution of $Li_6[BVW_{11}O_{40}]$ at 80 °C and directly measured $^2J_{W\text{-}O\text{-}V}$ = 7.4 Hz and $^2J_{W\text{-}O\text{-}V}$ = 25.9 Hz, in good agreement with the values from the fitted ^{183}W line shapes.

The $^2J_{W\text{-}O\text{-}V}$ values for all these compounds are collected in Table I. We have specifically included contributions due to ^{183}W isotopomer satellites in the fit but neglected the small coupling

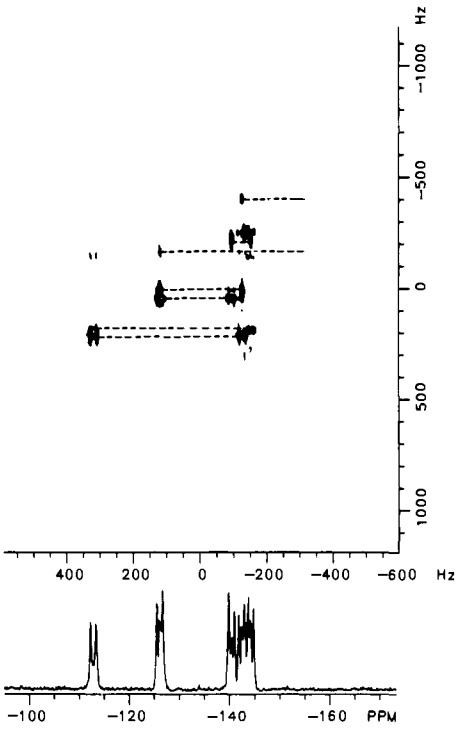

Figure 5. 2-D INADEQUATE ^{183}W NMR spectrum of ^{51}V-decoupled $Li_6[BVW_{11}O_{40}]$, 0.6 M, in D_2O, 30 °C, 640 transients, 128 files of 2048 words, 54 h, 20-mm sideways tube. Coupled sites are connected by horizontal lines at the sum frequency in the contour map. Some spectra show additional weak responses due to quadrature imbalance in the double quantum dimension (F_1). These are easily recognizable by their symmetrical disposition about $F_1 = 0$ with their strong real connection. For example, the weak response at $F_1 = -180$ Hz is an image of the strong connection at +180 Hz.

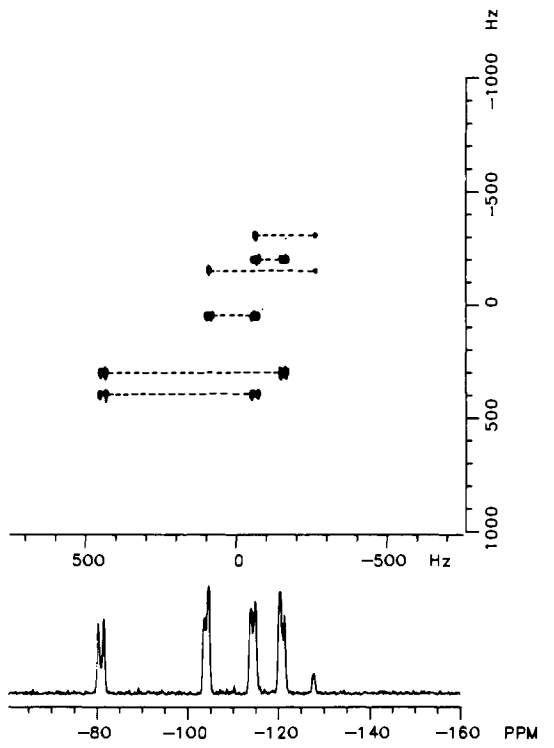

Figure 6. 2-D INADEQUATE ^{183}W NMR spectrum of ^{51}V-decoupled $Li_5[SiVW_{11}O_{40}]$, 0.6 M, 30 °C, 1536 transients, 128 × 2K files, 115 h, 20-mm sideways tube.

(1–2 Hz) due to ^{31}P and the vanishingly small[1] coupling with $^{11,10}B$. The significant aspect of these data is that $^2J_{W\text{-}O\text{-}V}$ is strongly dependent on the W–O–V bond angle in the same manner as $^2J_{W\text{-}O\text{-}W}$.[4] The connectivity arguments presented later show the lower J value corresponds to edge oxygen sharing of vanadium and tungsten octahedra while the larger J corresponds to a corner connection through oxygen. As a general rule, the broader ^{183}W resonances can be unambiguously assigned to a ^{51}V in an adjacent triad while the narrower lines contain ^{51}V and ^{183}W in the same edge-shared triad.

We can only speculate on the origin of the chemical exchange necessary to accurately fit the ^{183}W line shapes. Since $T_2(^{51}V)$ is independent of pH, anion concentration, and added VO_2^+, we believe the vanadium is not labile, unlike vanadomolybdate polyanions.[42] Brevard et al.[5a] have observed broadening of the ^{183}W line adjacent to Pb in a Keggin structure, and we have made similar observations in $[PZn(OH_2)W_{11}O_{39}]^{5-}$, indicating a dynamic process on the NMR time scale. Of course quadrupolar effects are ruled out in these latter compounds so we attribute the broadening to proton (or water) lability at the basic M–O–W sites. We are currently attempting to delineate the effect in $[PZnW_{11}O_{40}]^{7-}$ in nonaqueous, organic solvents. Our inability to determine a temperature dependence of the rate in XVW_{11} compounds over the range 20–80 °C reflects the small magnitude of the exchange relative to the effects of the quadrupole.

(d) 2-D Connectivity from ^{183}W NMR of Monosubstituted Anions. The 2-dimensional INADEQUATE spectra of $[BVW_{11}O_{40}]^{6-}$ and $[SiVW_{11}O_{40}]^{5-}$ are shown in Figures 5 and 6, respectively. Horizontal lines connect coupled sites. The magnitude of $^2J_{W\text{-}O\text{-}W}$ is clear from the contour map because the edge couplings ($J \sim 5$–12 Hz) appear as unresolved "ovals" because of the large line width whereas the larger couplings ($J \sim 15$–30 Hz) from corner connections produce "dumbbells" from all four resolved components of the AX spin systems. If necessary, individual rows of the matrix can be retrieved to measure the magnitude of $^2J_{W\text{-}O\text{-}W}$.

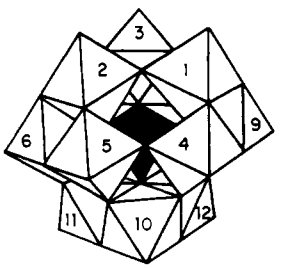

Figure 7. IUPAC numbering scheme of α-Keggin anions. Substituted vanadium atoms occupy sites 1 ($XVW_{11}O_{40}^{n-}$), 1 and 2 ($XV_2W_{10}O_{40}^{n-}$), and 1, 2, and 3 ($XV_3W_9O_{40}^{n-}$).

Figure 7 shows the IUPAC numbering scheme[31] of a polyhedral representation of the Keggin anion for use in the assignments. If vanadium occupies site 1, the following pairwise tungsten equivalences result: $W_2 = W_3$; $W_4 = W_9$; $W_5 = W_8$; $W_6 = W_7$; $W_{10} = W_{12}$. W_{11} is the unique tungsten. Expected couplings are tabulated in the tridiagonal matrix of Table II. Since W_{11} is easily assigned in $[BVW_{11}O_{40}]^{6-}$ on the basis of intensity we begin there; W_{11}, −140.7 ppm. The corner connection to W_6 (−126.4 ppm) is clearly distinguished from the edge connection to W_{10} (−144.5 ppm) which has a much smaller J coupling constant. W_6 shows edge connections to both W_5 and W_2. It is impossible to distinguish between W_2 and W_5 on this basis until we note W_{10} also has a corner connection back to W_5 and W_4. These arguments unambiguously identify W_5 (−142.8 ppm), W_2 (−154.8 ppm), and W_4 (−113.2 ppm). Of course, in retrospect, W_2 and W_4 could also have been assigned on the basis of their proximity to ^{51}V, and concomitant broadening, discussed earlier. Note that although W_2 is not observed directly in the projection of the 2-D spectrum, because of incomplete ^{51}V decoupling, the W_6–W_2 and W_5–W_2 connections are established from observation of only the W_6 and W_5 components, respectively, at the correct double quantum frequency.

Identical arguments can be applied to establishing the connectivity patterns in $[PVW_{11}O_{40}]^{4-}$ and $[SiVW_{11}O_{40}]^{5-}$, although in the latter case inexorable overlap of W_{11} and W_5 precludes beginning with the unique W_{11}. Complete assignments and

Table II. Connectivity Patterns Associated with α-$XVW_{11}O_{40}^{n-}$ and α-1,2-$XV_2W_{10}O_{40}^{n-}$ Species[a]

(a) $XVW_{11}O_{40}^{n-}$

V_1	$W_2(W_3)$	$W_4(W_9)$	$W_5(W_8)$	$W_6(W_7)$	$W_{10}(W_{12})$	W_{11}	
●	corner	edge	–	–	–	–	V_1
	●	–	edge	edge	–	–	W_2
		●	corner	–	corner	–	W_4
			●	edge	corner	–	W_5
				●	–	corner	W_6
					●	edge	W_{10}
						●	W_{11}

α-1,2-$XV_2W_{10}O_{40}^{n-}$

$V_1(V_2)$	W_3	$W_4(W_5)$	$W_6(W_9)$	$W_7(W_8)$	W_{10}	$W_{11}(W_{12})$	
●	corner	edge	edge	–	–	–	$V_1(V_2)$
	●	–	–	edge	–	–	W_3
		●	edge	–	corner	–	$W_4(W_5)$
			●	corner	–	corner	$W_6(W_9)$
				●	–	corner	$W_7(W_8)$
					●	edge	W_{10}
						●	$W_{11}(W_{12})$

[a] Numbering scheme from Figure 7.

Table III. Assignments of ^{183}W NMR Spectra of Polyvanadotungstates

	chemical shift/assignment[a]						
compound	$W_2(2)$	$W_4(2)$	$W_5(2)$	$W_6(2)$	$W_{10}(2)$	$W_{11}(1)$	center of gravity
$Li_6[BVW_{11}O_{40}]$ D_2O, 30 °C	−154.8	−113.2	−142.8	−126.4	−144.5	−140.7	−136.7
$Li_5[SiVW_{11}O_{40}]$ D_2O, 30 °C	−128.0	−81.1	−114.6	−104.3	−121.0	−114.6	−110.2
$Li_4[PVW_{11}O_{40}]$ D_2O, 30 °C	−106.7	−72.2	−101.2	−98.6	−108.7	−103.7	−98.1
$Li_7[PW_{11}O_{39}]$[b] D_2O, 35 °C	−98.8	−98.1	−132.4	−103.6	−152.2	−121.4	
$Na_8[SiW_{11}O_{39}]$[b] D_2O, 30 °C	−127.9	−116.1	−143.2	−100.8	−176.1	−121.3	
$Na_5[PPbW_{11}O_{40}]$ D_2O	−82.7	−74.4	−127.4	−102.8	−146.3	−111.5	−107.2
$(TBA)_5[PTiW_{11}O_{40}]$ CD_3CN	−109.2	−57.2	−106.7	−92.6	−118.0	−101.9	−97.2

	chemical shift/assignments[a]						
compound	$W_3(1)$	$W_4(2)$	$W_6(2)$	$W_7(2)$	$W_{10}(1)$	$W_{11}(2)$	center of gravity
α-1,2-$Li_6[SiV_2W_{10}O_{40}]$ D_2O, 30 °C	(−111.7)	−86.0	−83.5	−111.7	−142.5	−122.7	−106.2
α-1,2-$Li_5[PV_2W_{10}O_{40}]$ D_2O, 30 °C	(−91.9)	−80.8	−82.2	−106.7	−128.8	−116.7	−99.4

	chemical shift/assignments[a]		
compound	$W_4(6)$	$W_{10}(3)$	center of gravity
α-1,2,3-$Li_7[SiV_3W_9O_{40}]$ D_2O, 30 °C	−91.5	−136.7	−106.6
α-1,2,3-$Li_6[PV_3W_9O_{40}]$ D_2O, 30 °C	−86.6	−130.1	−101.1
$[(n\text{-}C_4H_9)_4N]_3[VW_5O_{19}]$ CD_3CN, 25 °C	+76.4 (4)	+75.9 (1)	76.3
$Li_4[V_2W_4O_{19}]$ D_2O, 30 °C	+70.3 (2)	+69.4 (2)	69.9

[a] Numbering scheme for Keggin ions shown in Figure 7. [b] From ref 5.

chemical shifts are collected in Table III. All other conceivable monosubstituted structures which have the correct integrated intensity pattern of 2:2:2:2:2:1 fail to provide a complete cyclic connectivity pattern. Therefore, assignment of these species as α-Keggin structures is unequivocal. Although this is an expected result in these simple species, similar connectivity arguments will be needed to resolve more complex structural types. Accurate integration of resonances is a necessary requirement but may result in an ambiguous structure.

It is instructive to compare the assignments of $[PVW_{11}O_{40}]^{4-}$ and $[SiVW_{11}O_{40}]^{5-}$ with their lacunary precursors $[PW_{11}O_{39}]^{7-}$ and $[SiW_{11}O_{39}]^{8-}$ recently reported by Brevard et al.[5a] Because of the different numbering schemes used, we have included their assignment, with our numberings, in Table III for ease of comparison. Clearly, there is no simple correlation between the chemical shifts of the same sites in the two sets of compounds. Vanadium substitution, with its concomitant line broadening or loss of signal, cannot be used as an assignment tool for the corresponding lacunary species in the case of Keggin ions.[3a] It has proven successful, however, in the assignment of P_2W_{17} species.[3b] If the broadened ^{183}W resonances adjacent to ^{51}V are *observed*, the line shapes can be used to assign them. Given the present poor level of understanding of the origin of different chemical shifts, each assignment must be made directly on the basis of tungsten–tungsten atom connectivities without recourse to indirect criteria.

One consistent feature observed in all spectra is that the tungsten resonance due to W_4, the site which edge shares two oxygen atoms with V(V), is consistently the most deshielded. We noted[7] a similar trend in $[PTiW_{11}O_{40}]^{5-}$ and Brevard et al.[5a]

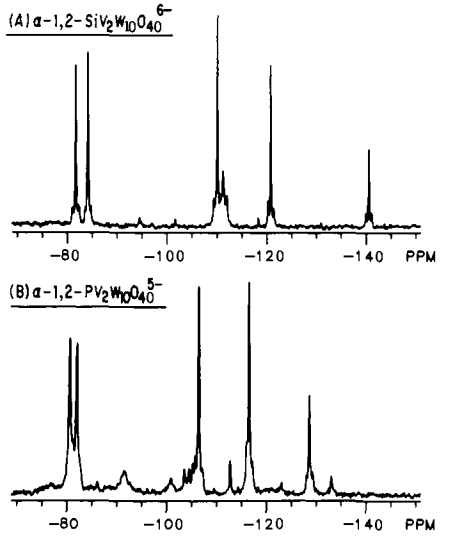

Figure 8. ^{51}V-decoupled 1-D ^{183}W NMR spectra of α-1,2-$K_6[SiV_2W_{10}O_{40}]$ and $Li_5[PV_2W_{10}O_{40}]$: (A) $K_6[SiV_2W_{10}O_{40}O]$, 0.2 M in D_2O, 30 °C, 32 768 transients, 19 h, 3-W ^{51}V decoupling, 20-mm sideways tube, LB = 1.0 Hz; (B) $Li_5[PV_2W_{10}O_{40}]$, 0.4 M in D_2O, 30 °C, 6284 transients, 1.8 h, 2-W ^{51}V decoupling, 20-mm sideways tube, LB = 2.0 Hz.

reported the same effect in $[PPbW_{11}O_{39}]^{5-}$. We (cautiously) propose this is a general phenomenon when WO^{4+} is replaced by an $MO^{(n-2)+}$ fragment of lower oxidation state, *n*. On the basis of Baker's arguments,[3a] these lines shift to high frequency because of increased electronic anisotropy around those tungsten atoms in the same triad. On the other hand, W_2, the tungsten atom sharing a corner in the adjacent triad, is uniformly shielded relative to the unsubstituted[3a] $[XW_{12}O_{40}]^{n-}$, although it is not always the lowest frequency line in the spectrum.

Tungsten W_6 is consistently the next-to-highest frequency line in all cases and is only slightly shifted from the parent XW_{12} resonance (B, −126.4 vs. −130.8; Si, −104.3 vs. −103.8; P, −98.6 vs. −99.4 for XVW_{11} vs. XW_{12}, respectively). The remaining chemical shifts of sites W_5, W_{10}, and W_{11} are too close to establish any relative ordering, but all are shielded relative to the parent. This overall distribution of chemical shifts produces a spectrum with the center of gravity close to the parent XW_{12} species.

(e) Disubstituted Keggin Anions. The conventional 1-D $^{183}W\{^{51}V\}$ spectra of α-1,2-$K_6[SiV_2W_{10}O_{40}]$ and α-1,2-$Li_5[PV_2W_{10}O_{40}]$ are shown in Figure 8. In the ^{51}V coupled spectra the pair of high-frequency lines are significantly broader signalling their proximity to ^{51}V. ^{51}V decoupling sharpens both these lines and the lower intensity resonance at −111 ppm (SiV_2W_{10}) and −92 ppm ($PV_2W_{10}O_{40}$). A related ^{183}W NMR spectrum of a different sample of $Li_6[SiV_2W_{10}O_{40}]$ shows no resolved line at −111 ppm indicating inexorable overlap with the stronger line.[32] These decoupling data, combined with the integrated intensities and 2-D connectivity plots, identify the −111 ppm (SiV_2W_{10}) and −92 ppm (PV_2W_{10}) lines as W_3 which corner shares *both* equivalent vanadium atoms and is thus difficult to completely decouple.

The integrated intensity pattern of the ^{183}W NMR spectrum and single-line ^{51}V NMR spectrum can be accounted for with *both* the 1,2- or 1,4-positional isomers of $[XV_2W_{10}O_{40}]^{n-}$. However, the 2-D connectivity maps (Figures 9 and 10) can only be rationalized for the 1,2 isomer. Following the expected connections (Table IIb) in $[SiV_2W_{10}O_{40}]^{6-}$, and beginning with W_{10}, which is assigned on the basis of intensity (−142.4 ppm), clear edge connections to W_{11} and W_{12} (−122.7 ppm) and corner connections to W_4 and W_5 (−86.0 ppm) define these sites. W_{11} shares two corners with W_6 and W_7 while W_4 and W_5 also share an edge with W_6. These combined arguments unambiguously define W_6, W_9 (−83.5 ppm) and W_7, W_8 (−111.7 ppm). The intensity of the contour reflecting corner coupling between W_6, W_9 (−83.5 ppm) and W_7, W_8 (−111.7 ppm) is lower because $^2J_{W\text{-}O\text{-}W}$ is not optimum for transfer into double quantum coherence. The single

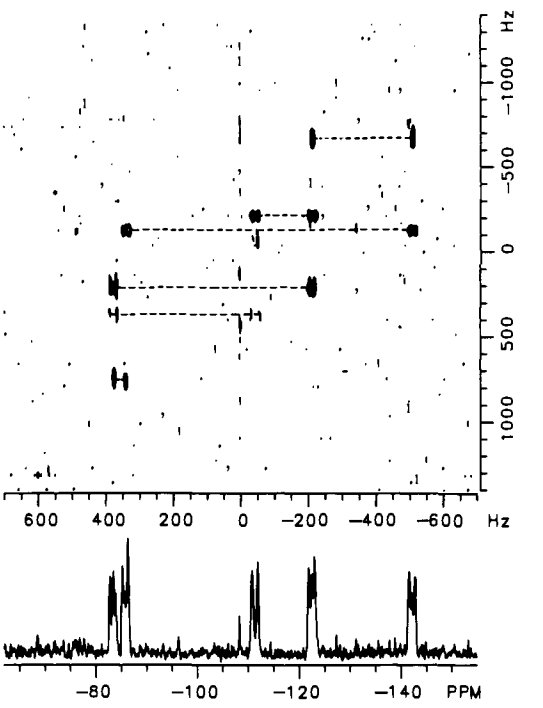

Figure 9. 2-D INADEQUATE ^{183}W NMR spectrum of ^{51}V-decoupled α-1,2-$Li_6[SiV_2W_{10}O_{40}]$, 0.4 M in D_2O, 30 °C, 1536 transients, 64 × 2K files, 96 h, 20-mm sideways tube. Note the contour at the intersection of −50 Hz (F_2) and −100 Hz (F_1). We believe this to be one component of a strongly coupled overlapped AB spin system of W_3 and W_7. (See text.)

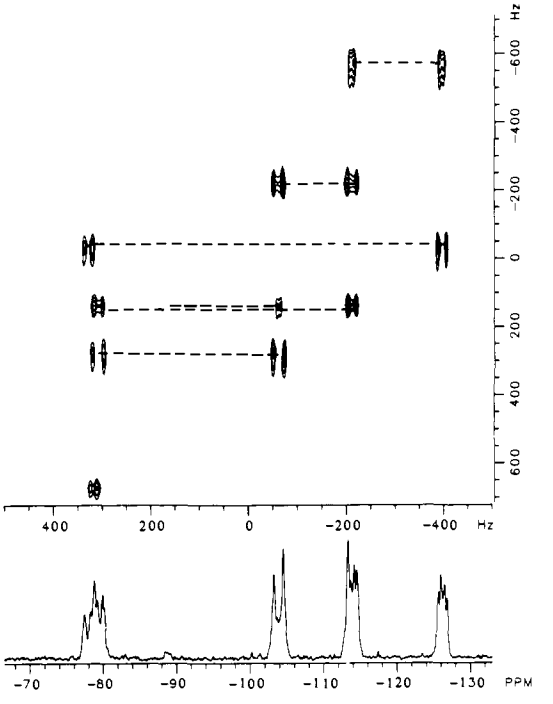

Figure 10. 2-D INADEQUATE ^{183}W NMR spectrum of ^{51}V-decoupled α-1,2-$Li_5[PV_2W_{10}O_{40}]$, 0.4 M in D_2O, 30 °C, 4096 transients, 32 × 2K files, 58 h, 20-mm sideways tube, 3.2-W ^{51}V decoupling.

contour observed at the intersection of −50 Hz (F_2) (−111.7 ppm) and −100 Hz (F_1) is a component of the W_7, W_8 – W_3 edge coupling in a highly second order AB pattern. Initial failure to identify this resonance caused confusion[32] in the identification of

(30) Abragam, A. "The Principles of Nuclear Magnetism"; Oxford University Press: Oxford, 1961.

(31) (a) Pope, M. T. "Heteropoly and Isopoly Oxometalates"; Jeannin, Y., Fournier, M., Eds.; Springer-Verlag: New York, 1983; Appendix. (b) Mossoba, M. M.; O'Connor, C. J.; Pope, M. T.; Sinn, E.; Herve, G.; Teze, A. *J. Am. Chem. Soc.* **1980**, *102*, 6864–6866.

this compound. The reasoning for all the assignments in $[PV_2W_{10}O_{40}]^{5-}$ is more straightforward because of superior data (Figure 10). In this case, the W_7, W_8 component of the W_7, W_8 – W_3 connection is clearly evident at −104 ppm but the W_3 component is weaker because of incomplete decoupling. $[PV_2W_{10}O_{40}]^{5-}$ has the same relative ordering of lines, as $[SiV_2W_{10}O_{40}]^{6-}$ except W_4, W_5 and W_6, W_9 are interchanged. Table III collects both sets of assignments. Application of these same arguments to the alternative 1,4-positional isomer fails. Pope has reported[31b] the ESR spectrum of the one electron reduced $[SiV^{V}V^{IV}W_{10}O_{40}]^{7-}$ and also suggested[32] it is the 1,2-positional isomer.

Again, it is noteworthy that the highest frequency lines W_6, W_9 and W_4, W_5 edge share vanadium. There is also a striking similarity in the overall pattern of ^{183}W NMR lines for the two homologous species. On the other hand, use of additivity rules between different species such as $[XVW_{11}O_{40}]^{n-}$ and $[XV_2W_{10}O_{40}]^{(n+1)-}$ is dangerous. On the basis of shifts in $[SiVW_{11}O_{40}]^{5-}$ and $[PVW_{11}O_{40}]^{4-}$ the W_3 resonance of both $[SiV_2W_{10}O_{40}]^{6-}$ and $[PV_2W_{10}O_{40}]^{5-}$ would be expected far upfield, which is not the case. The center of gravity is again close to the parent unsubstituted anion: −106.2 ppm for SiV_2W_{10} vs. −103.8 for SiW_{12}, −99.4 ppm for PV_2W_{10} vs. −99.4 ppm for PW_{12}.

(f) Trisubstituted Keggin Anions. Finke and co-workers[33] have studied the chemistry and ^{183}W NMR spectra of several trisubstituted silicotungstates, including A-α- and A-β-1,2,3-$[SiV_3W_9O_{40}]^{7-}$, generally as *tert*-butylammonium salts. Details of the ^{183}W NMR spectra depend on the extent of protonation, but in the fully protonated (or deprotonated) species the spectra are simply two lines of relative intensity 2:1 with the more intense line slightly broader than the other. Isotopomer satellites with $^2J_{W\text{-}O\text{-}W}$ = 15.7 ± 1.2 Hz confirm the A-type structure which is expected on the basis of the lacunary precursors[16,36] A-α- and A-β-$[SiW_9O_{34}]^{10-}$. Our ^{183}W NMR spectrum of the lithium salt α-1,2,3-$Li_7[SiV_3W_9O_{40}]$ shows the two lines at −91.5 ppm (intensity 6) and −136.7 ppm (intensity 3) ($^2J_{W\text{-}O\text{-}W}$ = 17.0 Hz).

α-1,2,3-$Li_6[PV_3W_9O_{40}]^{6-}$ has the same simple ^{183}W NMR spectrum with lines at −86.6 ppm (intensity 6) and −130.1 ppm (intensity 3) and $^2J_{W\text{-}O\text{-}W}$ = 16.8 Hz. The stronger line has a halfwidth of 5 Hz. These data are consistent with either α- or β-1,2,3-$[PV_3W_9O_{40}]^{6-}$ (60° rotation of the W_{10}, W_{11}, W_{12} triad) which cannot be distinguished. We favor the α form since the product can also be isolated from basic hydrolysis of α-$[PW_{12}O_{40}]^{3-}$ and subsequent treatment with stoichiometric quantities of $NaVO_3$; β-$[PW_{12}O_{40}]^{3-}$ is unknown.

The ^{183}W NMR lines of all the above species are relatively sharp due to edge sharing of vanadium and tungsten, with $^2J_{W\text{-}O\text{-}V} \sim$ 10 Hz, and the rapid relaxation of the ^{51}V lines ($\Delta\nu_{1/2} \sim 300$ Hz) which effectively decouples the two spins. ^{51}V decoupling is less effective since the decoupling field strength $\gamma H_2/2\pi$ is not large relative to $T_2^{-1}(^{51}V)$. 2-D spectra are not required because of the simplicity of the two-line spectrum.

(g) Hexametalate Isopolyanions. The ^{183}W NMR spectra of $[(n\text{-}C_4H_9)_4N]_3[VW_5O_{19}]$ and $Li_4[V_2W_4O_{19}]$ are quite broad in the absence of ^{51}V decoupling owing to the sharp ^{51}V lines observed because of shorter rotational correlation time in these smaller anions. The ^{51}V decoupled ^{183}W NMR spectrum of $[VW_5O_{19}]^{3-}$ shows two closely spaced lines of relative intensity 4:1 consistent with the proposed structure. The ^{51}V NMR resonance is sufficiently sharp that the ^{183}W satellites are observed with $^2J_{W\text{-}O\text{-}V}$ = 11.1 Hz.

$[V_2W_4O_{19}]^{4-}$ shows two equally intense ^{183}W lines consistent with the proposed cis structure.[34] No additional line attributable to a trans isomer was observed. Satellite isotopomer lines were not observed in either ^{183}W NMR spectrum because of close spacing, broad lines, and lower signal-to-noise ratios. NMR data are collected in Table III.

Table IV. ^{51}V NMR Parameters for $[V_{10}O_{28}]^{6-}$ and $[PV_{14}O_{42}]^{9-}$

compound	chemical shift, ppm	integral	line width, Hz	T_1, ms
$Na_6[V_{10}O_{28}]$	−423	2	370	0.7
in H_2O, 30 °C	−500	4	260	1.2
pH 4.5	−515	4	160	2.1
$Na_6[V_{10}O_{28}]$	−421	2	230	1.1
in H_2O, 60 °C	−497	4	160	1.9
pH 4.5	−513	4	110	3.4
$Na_8H[PV_{14}O_{42}]$	−526	2	230	
in H_2O, 60 °C	−577	8	350	
pH 2.4	−593	4	470	

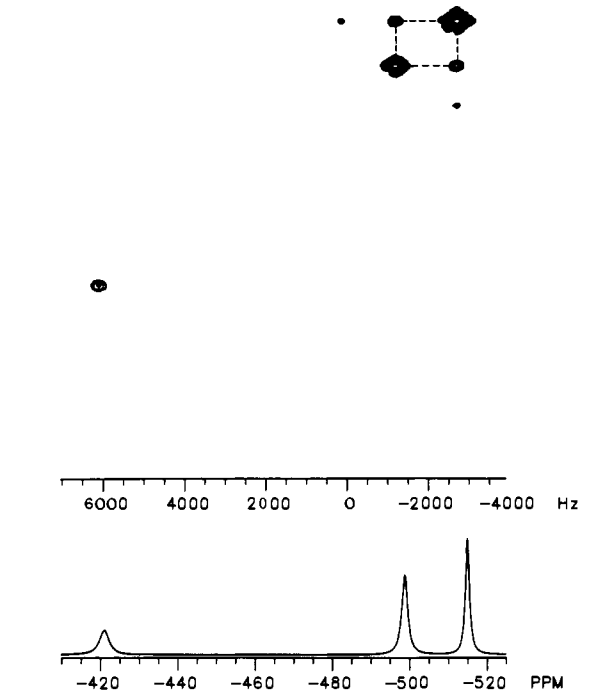

Figure 11. 2-D ^{51}V–^{51}V COSY spectrum of $Na_{6-x}H_x[V_{10}O_{28}]$ at pH 4.5, 60 °C. The lower portion contains a conventional 1-D ^{51}V NMR spectrum. The sample was a saturated 25 °C solution (see Experimental Section), 7680 transients, 256 × 512 files, 11 h. Correlations between sites with shifts of δ_1 and δ_2 appear as off-diagonal peaks at (δ_1, δ_2) and (δ_2, δ_1).

(h) 2-D Connectivity Patterns in $V_{10}O_{28}^{6-}$ and $PV_{14}O_{42}^{9-}$. ^{51}V NMR has proven to be a valuable technique for detection of solution species of iso- and heteropolyanions.[35] The principal drawback is that the broad lines generally obscure spin–spin coupling. Information on atom–atom connectivities is thus lacking. Encouraged by recent reports of 2-D *J*-correlated (COSY90) NMR studies of ^{11}B in cluster compounds,[36] we sought to establish connectivities in oxovanadates by similar means.

The compounds chosen as representative models were[35,20] $V_{10}O_{28}^{6-}$ and $PV_{14}O_{42}^{9-}$. Spectral parameters including chemical shifts, line widths, relative intensities, and T_1 relaxation times are collected in Table IV. The similarity of T_1 and $T_2 = (\pi\Delta\nu_{1/2})^{-1}$ indicates only small couplings are expected. Also, the magnitudes of $^2J_{V\text{-}O\text{-}W}$ and $^2J_{W\text{-}O\text{-}W}$ found in Keggin structures suggest $^2J_{V\text{-}O\text{-}V} \sim$ 5–25 Hz. Conventional ^{51}V NMR spectra of both compounds show no evidence of spin–spin coupling even after resolution

(32) Early observations were initially interpreted as the species being $[SiV_2W_9O_{39}]^{10-}$, but the ^{51}V NMR chemical shift was similar to that reported by Pope[31b] for $[SiV_2W_{10}O_{40}]^{6-}$. Indeed, exchange of compounds confirmed the species were identical (^{51}V NMR, ESR, electrochemistry). Analysis also showed only 6 potassium counterions. We are grateful to Professor Pope and M. Leparulo for correspondence and cooperation in resolving this difference. See remaining text.

(33) Finke, R. G.; Rapko, B., private communication.

(34) (a) Nishikawa, K.; Kobayashi, A.; Sasaki, Y. *Bull. Chem. Soc. Jpn.* **1975**, *48*, 889–892. (b) Klemperer, W. G.; Shum, W. *J. Am. Chem. Soc.* **1978**, *100*, 4891–4893.

(35) See, for example: O'Donnell, S. E.; Pope, M. T. *J. Chem. Soc. Dalton Trans.* **1976**, 2290–2297.

(36) (a) Venable, T. L.; Hutton, W. C.; Grimes, R. N. *J. Am. Chem. Soc.* **1982**, *104*, 4716–4717. (b) Venable, T. L.; Hutton, W. C.; Grimes, R. N. *J. Am. Chem. Soc.* **1984**, *106*, 29–37.

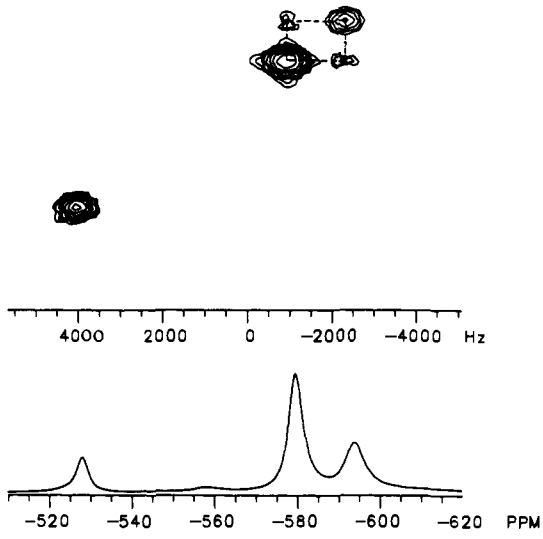

Figure 12. 2-D $^{51}V-^{51}V$ COSY spectrum of $Na_{9-x}H_x[PV_{14}O_{42}]$ at (0.07 M) pH 1.7, 60 °C, 40960 transients, 128 × 256 files, 9.1 h.

enhancement of high signal-to-noise ratio data. The problem is then a "worst case" for detection of a V–O–V connectivity pattern.

Figures 11 and 12 show the 2-D COSY90 spectra of both compounds. In these contour plots diagonal elements (45°) represent a normal chemical shift spectrum of inequivalent sites while off-diagonal elements are due to $^2J_{V-O-V}$ coupling between adjacent sites. $[PV_{14}O_{42}]^{9-}$ clearly shows a correlation between the lowest frequency peaks at −577 and −593 ppm. Integration of these peaks (8:4) shows they are due to the main Keggin framework. On the other hand, no off-diagonal peak exists between the capping vanadium at −526 ppm and the adjacent atoms in the Keggin structure. Similarly, only one of the three possible correlations is observed in $[V_{10}O_{28}]^{6-}$. Some considerable effort was made to observe these connections by varying the coherence transfer times.[25] The correlations that are observed are very weak and approach the spectrometer artifact levels. Nevertheless, the detection of the connectivity pattern in broad featureless spectra is an important feat; an inherent resolution problem has been converted to a sensitivity problem. The significant aspect of the result is that connectivity in Keggin anions can be determined because the magnitude of $^2J_{V-O-V}$ is favorable. Presumably as $^2J_{V-O-V}$ decreases with decreasing V–O–V angle the sensitivity problem becomes more severe because of the short T_2 relative to $(^2J_{V-O-V})^{-1}$.

Summary and Discussion

Specific positional isomers of vanadotungstate Keggin compounds can be prepared in simple reactions of precursor lacunary anions with VO^{2+} and VO_3^-. Unfortunately, not all the precursors are well characterized in the literature. The A-type structure of β-$[SiW_9O_{34}]^{10-}$ is unambiguously established from X-ray crystallography,[37] but for the analogous α-$[SiW_9O_{34}]^{10-}$ the A-form is inferred on the basis of similar chemistry[16,41] and polarography. Both α- and β-$[PW_9O_{34}]^{9-}$ are reported[38,39] although the preparative route to only β-$[PW_9O_{34}]^{9-}$ is described.[18] There is no definitive evidence to favor an A- or B-type structure. The α-1,2-V_2W_{10} and α-1,2,3-V_3W_9 isomers of both Si and P described here are derived from literature preparations[16,18] of α-$[SiW_9O_{34}]^{10-}$ and β-$[PW_9O_{34}]^{9-}$ and are based upon the A-type structure. The reaction to produce α-1,2,3-$[PV_3W_9O_{40}]^{6-}$ proceeds slowly over a period of 24 h and slow, solution isomerization (A → B) of the precursor cannot be ruled out. However, the reaction to give α-1,2-$[PV^{IV}_2W_{10}O_{40}]^{7-}$ appears complete in 30 min and maintains high specificity for the 1,2-isomer. While products of subsequent reactions cannot provide unambiguous proof of a precursor structure, we favor formulation of $Na_8H[PW_9O_{34}]$ as an A-type entity on this basis. Note, however, that products reported by Finke et al.[9] and Tourne et al.[39] are based upon a B-α-PW_9 structure. The more recent work[9] notes that heating is necessary to produce their structure, presumably forcing an A → B isomerization.

The reaction to produce α-1,2,3-$[PV_3W_9O_{40}]^{6-}$ proceeds with 3 equiv of metavanadate in a buffered solution at pH 4-8-5.2, where $[PW_{11}O_{39}]^{7-}$ is known to exist. Indeed, reaction of $Li_7[PW_{11}O_{39}]$ with excess metavanadate produces the same product, although less pure. The normal high isomeric purity of the product is lost if the reaction is heated, suggesting a thermodynamic minimum on the potential surface.

The reaction of $[PW_9O_{34}]^{9-}$ with 2 equiv of $VOSO_4$ produces V_1W_{11}, V_2W_{10}, and V_3W_9 in the crude reaction mixture after oxidation with Br_2. Precipitation with KCl results in the V_2W_{10} product almost exclusively. Separation of the different species is feasible because of their different solubilities.

α-1,2-$[SiV_2W_{10}O_{40}]^{6-}$ and α-1,2,3-$[SiV_3W_9O_{40}]^{7-}$ have been reported very recently.[31b] Our isolation of products from reaction of VO_3^- or VO^{2+} with α-$[SiW_9O_{34}]^{10-}$ parallels that of the $[PW_9O_{34}]^{9-}$ reaction. Solubility differences between the two species allows their separation.

In all the above chemistry ^{51}V NMR provided a necessary, and convenient, monitor of the syntheses through both chemical shift and line width information. Line widths increase substantially in the order α-XVW_{11} < α-1,2-XV_2W_{10} < α-1,2,3-XV_3W_9, for example, PVW_{11}, 26 Hz; PV_2W_{10}, 122 Hz; PV_3W_9, 275 Hz and $SiVW_{11}$, 33 Hz; SiV_2W_{10}, 116 Hz; SiV_3W_9, 320 Hz. Chemical shifts may be strongly pH dependent because of protonation of the more basic V–O–V sites, for example, in PV_3W_9, δ −532.5 ppm, pH 5.7; δ −553.8, pH 1.6. Pope and Leparulo[40] have made similar observations in a more extensive study.

The ^{183}W NMR studies described were undertaken for structure verification of the synthesized anions. Complete connectivity patterns for XVW_{11} (X = B, Si, P) anions confirm they are based upon the α-Keggin structure whereas simple integrated intensities are ambiguous. Corresponding patterns for XV_2W_{10} (X = Si, P) prove that only the α-1,2 positional isomer has been isolated, and simple 1-D spectra of XV_3W_9 (X = Si, P) show them to be exclusively the α-1,2,3-isomers. That these definitive statements of structure can be made attest to the power of ^{183}W NMR as a structural tool in polymetalate chemistry. In all cases the two bond $^2J_{W-O-W}$ couplings, and integrated band intensities, are the sole basis for determination of the structure. Earlier arguments,[3a] using the *disappearance* of lines adjacent to quadrupolar ^{51}V as an assignment tool for lacunary Keggin ions, are shown to be incorrect. The method is, however, vindicated in the case of P_2W_{17} species.[3b] The center of gravity of the ^{183}W NMR spectra remain relatively constant for a given heteroatom, and the relative distribution of lines is much the same for a homologous series, producing a remarkable similarity in the qualitative appearance of the spectra. One feature in all spectra is that tungsten atoms in the same triad as the substituent are consistently the most deshielded.

Quantitative treatment of the ^{183}W NMR line shapes of sites adjacent to the quadrupolar ^{51}V show that the two-bond $^2J_{W-O-V}$ coupling constants parallel those observed for $^2J_{W-O-W}$. Smaller J values are observed for *intra*group couplings with M–O–M angles of 120° whereas larger values result from *extra*group couplings where M–O–M angles of 150° are typical.[4] The effect of these differences is that tungsten atoms in the same triad as vanadium have considerably sharper lines than those in the ad-

(37) Robert, F.; Teze, A. *Acta. Crystallogr.* **1981**, *837*, 318–322.
(38) Contant, R.; Fruchart, J. M.; Herve, G.; Teze, A. *C. R. Hebd. Seances Acad. Sci., Ser. C* **1974**, *278*, 199–202.
(39) Tourne, C.; Revel, A.; Tourne, G.; Vendrell, M. *C. R. Hebd. Seances Acad. Sci., Ser. C* **1973**, *277*, 643–645.
(40) Pope, M. T.; Leparulo, M., private communication.
(41) Solid-state ^{29}Si NMR spectra show lines at −84.6 ppm with a shoulder at −83.6 ppm for A-α-$[SiW_9O_{34}]^{10-}$ and −83 ± 1 ppm for A-β-$[SiW_9O_{34}]^{10-}$. The same relative ordering of ^{29}Si resonances is observed in solution spectra of A-α-$[SiV_3W_9O_{40}]^{7-}$ (−84.4 ppm) and A-β-$[SiV_3W_9O_{40}]^{7-}$ (−83.7 ppm). We thank R. D. Farlee for recording the solid-state NMR spectra.
(42) Matveev, K. I.; Kozhevnikov, I. V. *Kinet. Catal.* (*Engl. Transl.*) **1980**, *21*, 855–863.

joining triad, and assignments are possible by inspection. Narrowest ^{183}W NMR lines result from the broadest ^{51}V resonances which in turn stem from high-viscosity solutions at low temperature.

Finally, 2-D ^{51}V J-correlation spectroscopy (COSY) extends the concept of measuring metal–metal atom connectivity patterns to quadrupolar nuclei. Although not all possible connections are observed due to the small magnitude of $^2J_{V-O-V}$ relative to T_2^{-1}, adjacent locations in the Keggin structure are easily detectable. These data complement ^{183}W–^{183}W atom connectivities and will prove to be a useful structural tool in higher vanadium substituted species.

Acknowledgment. I am grateful to Professor M. T. Pope and M. Leparulo for sharing information and providing a sample of $[SiV^{IV}_2W_{10}O_{40}]^{8-}$ for comparison with our compounds. Professor R. G. Finke and B. Rapko kindly supplied details of their synthesis of β-$[SiV_3W_9O_{40}]^{7-}$. I also thank W. H. Knoth for stimulating discussions. G. Watunya, J. Jensen, and J. T. Seningen provided skilled technical assistance.

Saturated and Polymerizable Amphiphiles with Fluorocarbon Chains. Investigation in Monolayers and Liposomes

R. Elbert, T. Folda, and H. Ringsdorf*

Contribution from the Institute of Organic Chemistry, University of Mainz, D-6500 Mainz, Federal Republic of Germany. *Received March 6, 1984*

Abstract: The synthesis and characterization of several saturated and polymerizable amphiphiles with fluorocarbon chains are described. Monolayers of lipids containing fluorocarbon chains are more stable than those formed from their hydrocarbon counterparts. The creation of phase-separated monolayers and liposomes is possible when the membrane is composed of a mixture of lipids containing hydrocarbon chains and lipids containing fluorocarbon chains. Phase separation even occurs when the two lipids bear the same head group. Complete phase separation of a natural lipid (DMPC) and a lipid with fluorocarbon chains, **1**, could be demonstrated in liposomes by using freeze-fracture electron microscopy. Phase separation was even confirmed when the percentage of the fluorocarbon amphiphile was as low as 5 mol %. The polymerization behavior of unsaturated amphiphiles with fluorocarbon chains was investigated in monolayers and liposomes. The polymerization in liposomes could be followed by UV spectroscopy. Preservation of the spherical structure of the polymeric vesicles is demonstrated by electron microscopy.

Monolayers, black lipid membranes, and liposomes from natural and synthetic lipids are of interest as models for biological membranes. In addition, the polymerization of lipid molecules containing 1,3-butadiyne,[1-3] butadiene,[4] methacrylate, or acrylate[4-6] moieties as polymerizable groups leads to more stable model membranes. Nearly all amphiphiles investigated so far in this connection contain hydrocarbon chains as a hydrophobic moiety.

Perfluorocarbons are known to have physical properties which differ from their hydrocarbon analogues and often are immiscible with hydrocarbons.[7,8] Tensids containing fluorocarbon chains are known to have critical micelle concentrations similar to comparable hydrocarbon surfactants containing a 50% longer alkyl chain.[9] The greater hydrophobicity of a CF_2 group compared to a CH_2 group and the limited miscibility of fluorocarbon and hydrocarbon amphiphiles in micelles[10] were the reasons for the recent investigation of liposome-forming amphiphiles containing fluorocarbon chains.[11]

In this publication the synthesis of both saturated and polymerizable fluorine-containing amphiphiles and their behavior in monolayers and liposomes are described. As in the case of hydrocarbon lipids, the polymerization of fluorocarbon amphiphiles could be expected to enhance the stability of such model membranes. The mixing behavior of lipids with hydrocarbon and

Table I. Structure and Melting Points of Fluorocarbon and Hydrocarbon Amphiphiles

no.	compound	melting point, °C
1	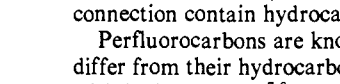	38
2	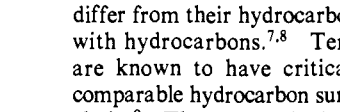	124
3	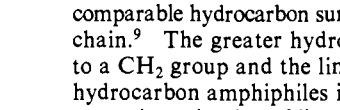	160–161
4	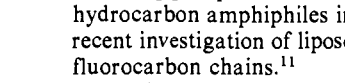	116
5	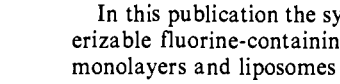	142[23]
6	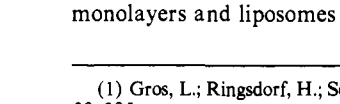	108
7	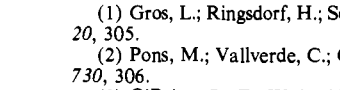	49
8	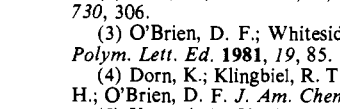	66
9	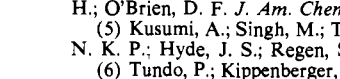	88[25]
10	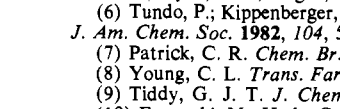	79–80

(1) Gros, L.; Ringsdorf, H.; Schupp, H. *Angew. Chem. Int. Ed. Engl.* **1981**, *20*, 305.
(2) Pons, M.; Vallverde, C.; Chapman, D. *Biochim. Biophys. Acta* **1983**, *730*, 306.
(3) O'Brien, D. F.; Whitesides, T. H.; Klingbiel, R. T. *J. Polym. Sci., Polym. Lett. Ed.* **1981**, *19*, 85.
(4) Dorn, K.; Klingbiel, R. T.; Specht, D. P.; Tyminski, P. N.; Ringsdorf, H.; O'Brien, D. F. *J. Am. Chem. Soc.* **1984**, *106*, 1627.
(5) Kusumi, A.; Singh, M.; Tirrell, D. A.; Oehme, G.; Singh, A.; Samuel N. K. P.; Hyde, J. S.; Regen, S. L. *J. Am. Chem. Soc.* **1983**, *105*, 2975.
(6) Tundo, P.; Kippenberger, D. J.; Politi, M. J.; Klahn, P.; Fendler, J. H. *J. Am. Chem. Soc.* **1982**, *104*, 5352.
(7) Patrick, C. R. *Chem. Br.* **1971**, *7*, 154.
(8) Young, C. L. *Trans. Faraday Soc.* **1969**, *65*, 2639.
(9) Tiddy, G. J. T. *J. Chem. Soc., Faraday Trans. 1*, **1972**, *68*, 369.
(10) Funasaki, N.; Hada, S. *J. Phys. Chem.* **1980**, *84*, 1868.
(11) Kunitake, T.; Okahata, Y.; Yasunami, S. *J. Am. Chem. Soc.* **1982**, *104*, 5547.

0002-7863/84/1506-7687$01.50/0